ARTICLES
https://doi.org/10.1038/s41567-019-0762-7

nature physics

Echo in a single vibrationally excited molecule

Junjie Qiang[1,5], Ilia Tutunnikov[2,5], Peifen Lu[1], Kang Lin[1], Wenbin Zhang[1], Fenghao Sun[1], Yaron Silberberg[3], Yehiam Prior[1,2*], Ilya Sh. Averbukh[2*] and Jian Wu[1,4*]

Echoes occur in many physical systems, typically in inhomogeneously broadened ensembles of nonlinear objects. They are often used to eliminate the effects of dephasing caused by interactions with the environment as well as to enable the observation of proper, inherent object properties. Here, we report the experimental observation of quantum wave-packet echoes in a single, isolated molecule. The entire dephasing–rephasing cycle occurs without any inhomogeneous spread of molecular properties, or any interaction with the environment, and offers a way to probe the internal coherent dynamics of single molecules. In our experiments, we impulsively excite a vibrational wave packet in an anharmonic molecular potential and observe its oscillations and eventual dispersion with time. A second, delayed pulse gives rise to an echo—a partial recovery of the initial coherent oscillations. The vibrational dynamics of single molecules is visualized by a time-delayed probe pulse dissociating them, one at a time. Two mechanisms for the echo formation are discussed: a.c. Stark-induced molecular potential shaking and creation of a depletion-induced 'hole' in the nuclear spatial distribution. The single-molecule wave-packet echoes may lead to the development of new tools for probing ultrafast intramolecular processes in various molecules.

Echoes in physical systems were introduced by Erwin Hahn in 1950[1,2] within the framework of spins embedded in an inhomogeneous environment. They are typically used to measure dephasing rates on the basis of the local interaction of the spins with their surroundings. Following the original discovery of echoes in ensembles of spins excited by pulsed magnetic fields, many different types of echo have been observed, including photon echoes[3,4] and their mechanical analogues[5]—cyclotron echoes[6], plasma-wave echoes[7], cold atom echoes in optical traps[8–10], echoes in cavity quantum electrodynamics[11], echoes in particle accelerators[12–15] and, more recently, echoes in a gas of rotating molecules[16–21]. In general, an ensemble of nonlinear objects (spins, molecules, plasma, a beam of particles and so on), when impulsively excited by an external stimulus, results in a prompt coherent response. Because each member of the ensemble evolves at a different frequency, the response disappears as the members of the ensemble step out of phase. However, and this is the essence of the echo phenomenon, the effect of the first excitation is not lost, and it is possible to retrieve it. By applying a second pulsed excitation and waiting a time period equal to the delay between the two excitations, a response signal emerges again, and is referred to as an 'echo'. In general (but not in our case, see below), the interaction with the environment causes a loss of coherence and reduces the echo signal amplitude. This reduction in echo amplitude provides information on the environmentally induced decoherence. The echo in an ensemble of nonlinear objects should be distinguished from quantum revivals. In contrast to echoes, the quantum revivals appear after a single-pulse excitation, and their period depends only on the intrinsic properties of the energy spectrum[22–25].

In parallel with this interest in echoes, single-molecule spectroscopy has drawn an increasing level of attention since the seminal works in refs. [26,27], eventually leading to super-resolution and super-sensitive optical microscopy, where single molecules embedded in thin films are selected spectrally by narrowband continuous-wave (c.w.) lasers within homogeneously broadened lines, or isolated spatially by observing dilute samples where only one molecule lies within the field of view of the microscope. An alternative approach to observing single molecules is to measure them while embedded within individual quantum dots, and then spectral or spatial resolutions are not required, enabling time-domain experiments[28,29]. Ultrafast experiments based on sensitive fluorescence detection have allowed the observation of various coherent excitations of vibrational wave packets in single molecules[30] (for a review see ref. [31] and a more recent work[32], as well as references therein). Coherent oscillatory signals from molecular vibrational wave packets impulsively excited by short pulses are typically washed out on the femtosecond timescale after several oscillations. This collapse of the coherent transients originates from intramolecular dephasing of multiple vibrational states forming the wave packet in a single molecule. This is actually a quantum phenomenon, as oscillations of a single nonlinear classical oscillator never collapse, and last 'forever'.

The other type of 'single particle experiment' is typically an interference experiment where single electrons, or single photons, pass through a double slit, one at a time[33,34], and the probability of hitting the screen at a specific location is provided by quantum mechanics. The probability distribution can be derived by repeating the measurement many times, each time with a new single particle. These experiments are known as 'single particle' interference experiments, and this is exactly the type of experiment we are presenting here, but in our case the interference happens in the time domain. The molecules interact with the laser fields one at a time and are individually measured. As in similar experiments, to see the distributions, the measurement is repeated many times.

Here, we show that it is possible to partially overcome the effects of intramolecular dephasing and cause the coherent oscillations to recur by inducing an echo in a single isolated molecule. We report the experimental observation of the quantum wave-packet echo (WPE) at the level of a single molecule, and provide a detailed theoretical analysis of this phenomenon. In our experiments, using an

[1]State Key Laboratory of Precision Spectroscopy, East China Normal University, Shanghai, China. [2]AMOS and Department of Chemical and Biological Physics, Weizmann Institute of Science, Rehovot, Israel. [3]AMOS and Department of Physics of Complex Systems, Weizmann Institute of Science, Rehovot, Israel. [4]Collaborative Innovation Center of Extreme Optics, Shanxi University, Taiyuan, Shanxi, China. [5]These authors contributed equally: Junjie Qiang, Ilia Tutunnikov. *e-mail: yehiam.prior@weizmann.ac.il; ilya.averbukh@weizmann.ac.il; jwu@phy.ecnu.edu.cn

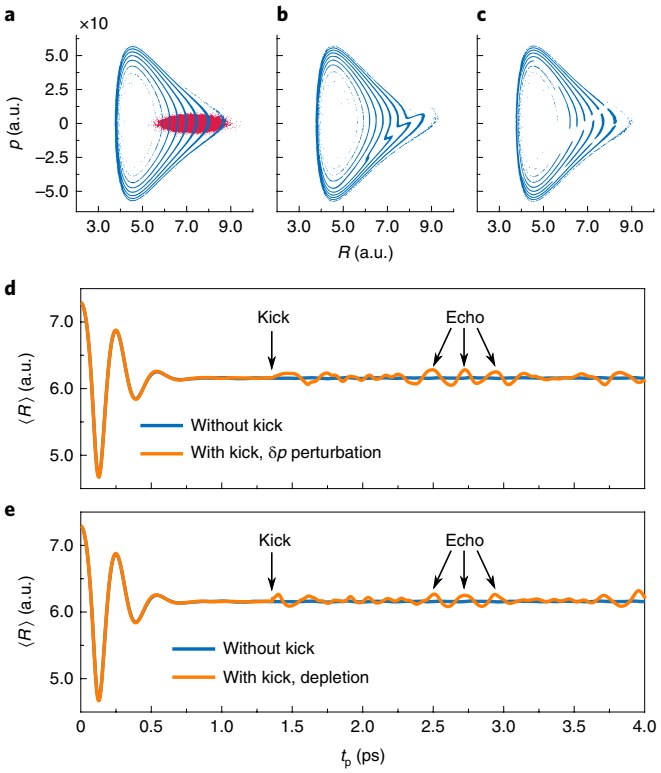

Fig. 1 | Classical phase space dynamics. The temporal evolution of the non-equilibrium phase space distribution $\rho_0 \propto \exp(-(R-R_0)^2/2\sigma^2)\exp(-\sigma^2 p^2/2)$, where R_0 is the equilibrium bond length of Ar_2 and σ^2 is the ground-state coordinate variance of Ar_2 (obtained by a Gaussian function fit). The evolution was simulated by the Monte Carlo approach using an ensemble of $N = 10^5$ molecules. **a**, Initial phase space distribution (in red) and filamented distribution just before the kick at $t_k = 1.36$ ps (in blue). **b**, The distribution shortly after a kick implemented by a uniform momentum increment in each molecule by $\delta p = 1$a.u. **c**, The distribution shortly after a kick implemented by removing all the molecules within the strip of 5.5 a.u. $< R <$ 6.1 a.u. **d**,**e**, The ensemble-averaged interatomic separation $\langle R\rangle(t)$ and the echo response at $t \approx 2t_k$ without (blue curve) and with (orange curve) a kick for the case of the δp perturbation (**d**; also see **b**) and the case with particle depletion (**e**; also see **c**).

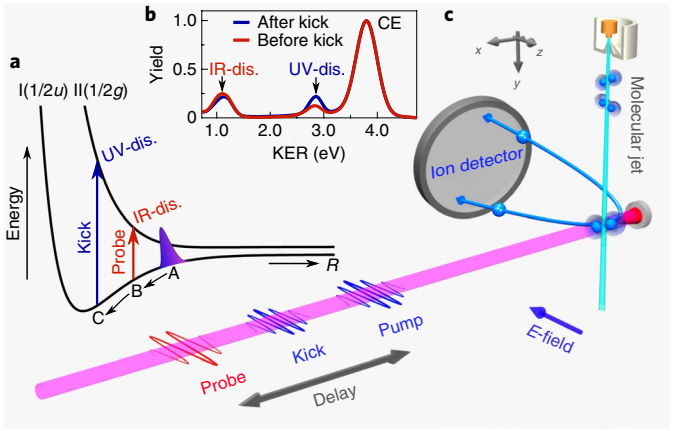

Fig. 2 | Experimental set-up. a, A coherent nuclear wave packet is launched by the pump pulse, which excites a neutral argon dimer Ar_2 (not shown) to the $I(1/2u)$ potential of the ion Ar_2^+ at point A. The wave packet oscillates in the bound $I(1/2u)$ potential, and is later dissociated by excitation of the ion to the dissociating $II(1/2g)$ potential. The excitation to the $II(1/2g)$ state is done by either the probe pulse (790 nm) at point B or by the kick pulse (395 nm) at point C. **b**, These pulses lead to dissociation via the $Ar_2(1, 0)$ channel with different KER ranging from 0.7 to 3.2 eV, where 'IR-dis.' and 'UV-dis.' refer to dissociation induced by 790 nm and 395 nm pulses, respectively. At higher energies, close to 4 eV, the Coulomb explosion (CE) peak is visible, corresponding to the double ionization process. **c**, Schematic of the experimental apparatus.

ultrashort femtosecond laser pulse, we create a localized vibrational wave packet in an argon dimer cation. This wave packet oscillates back and forth in the ion potential well and disperses completely due to the spread of the oscillation frequencies within the wave packet. Next, after a time delay of t_k, a second laser pulse is applied. We demonstrate that an impulsive molecular response (echo) indeed emerges at time $2t_k$ as a result of the rephasing of the components of the wave packet. The entire sequence of excitation, dispersion, re-excitation and the WPE occurs within a single isolated molecule. The ability to observe a single-molecule event stems from our detection methodology COLTRIMS (cold target recoil ion momentum spectroscopy)[35,36], where the fragments of every single molecule are individually detected following its dissociation. The observed WPE is a generic phenomenon that can, in principle, be observed by imaging nuclear dynamics in a variety of molecules[37,38] and in other impulsively excited isolated quantum systems. Our choice of weakly bound argon dimers is motivated by their relatively low vibrational frequencies, as this simplifies the time-resolved measurements.

Classical counterpart of the quantum WPE

Although the vibrational WPE in a single molecule is a quantum phenomenon, a classical phase space analysis of the evolution of an ensemble of molecules after impulsive excitation provides useful insights into the mechanism of the echo formation. With this qualifying remark in mind, we now consider the vibrational dynamics in an ensemble of non-interacting homonuclear diatomic molecules. The vibrational motion of each molecule is modelled as motion of a classical point particle having mass $M/2$ (where M is the mass of each atom) in a one-dimensional (1D) anharmonic potential, $V(R)$. Motivated by our experiments, we consider the $I(1/2u)$ potential of the argon dimer cation Ar_2^+, which has its equilibrium internuclear distance at $R_0^+ = 4.56$ a.u. The Hamiltonian governing the motion of each molecule is $\mathcal{H}(p,R) = p^2/M + V(R)$, where p is the momentum associated with the coordinate R. To imitate the initial state created by an instantaneous ionization of Ar_2, the initial phase space distribution mimics the ground state of the neutral Ar_2 (Fig. 1a, red).

In an anharmonic potential, the frequency (period) of oscillations is energy-dependent. As a result, with time, the initial smooth phase space distribution (Fig. 1a, red) evolves into a spiral-like structure and gradually fills the accessible phase space (Fig. 1a, light blue). This filamentation of the phase space results in an increasing number of spiral turns, which become thinner to conserve the volume. A similar effect is known in stellar systems[39] and in accelerator physics[40]. To induce the echo response, a second excitation ('kick') is applied at $t = t_k$ when the filamentation is well developed. In our experiments, the kick is provided by an ultrashort laser pulse that disturbs the molecules in two ways: (1) it instantaneously changes the nuclei momentum due to the coordinate-dependent a.c. Stark shift of the molecular potential and (2) it transfers a fraction of the ion ground-state molecules to the excited electronic state via the optical absorption process. In the latter case, the kick drills a 'hole' in the spatial distribution (a vertical strip in the phase space distribution), centred at the resonance position[41]. We consider the two mechanisms separately and show that both lead to a subsequent echo response at $t = 2t_k$, as shown in Fig. 1d,e.

In the first mechanism, a kick caused by a coordinate-dependent a.c. Stark shift of the molecular electronic terms is modelled by an instantaneous uniform addition of momentum δp to all molecules. The kick is followed by formation of sharp 'tips' on each branch of the spiral (Fig. 1b). Due to the spread in their relative velocities in the anharmonic potential, the tips desynchronize with time. Here, we use the ensemble-averaged time-dependent internuclear separation, $\langle R\rangle(t)$, as an indicator for the distribution spreading. The initial filamentation of the phase space leads to decaying oscillations of $\langle R\rangle(t)$ as the distribution spreads. The kick at $t=t_k$ gives rise to an instantaneous response in $\langle R\rangle(t)$ that then decays as well, but at time $t\approx 2t_k$ the tips meet again, resulting in a transient spatial inhomogeneity, and an echo signal can be clearly observed (Fig. 1d). The described mechanism is similar to the one responsible for formation of the transverse beam echoes predicted and observed in particle accelerators[12–15].

In the second mechanism, we assume that the kick depletes the population in some spatial interval, but does not affect the vibrational motion. In other words, the pulse carves out a strip from the phase space distribution by instantaneously removing all the particles within this strip. This process mimics optical absorption and creates a 'hole' on each branch of the spiral. Figure 1c shows the phase space distribution shortly after instantaneous depletion. These holes move relative to each other and desynchronize with time (similar to the tips discussed in the previous paragraph). As before, the holes meet again at $t=2t_k$, leading to the echo response. Figure 1e shows the echo signal induced by the second mechanism.

This classical phase space analysis sheds light on the origin of the echo and suggests the two mechanisms leading to its formation. The results of a full quantum mechanical simulation are presented in the section 'Quantum mechanical analysis of the WPE'.

Experimental methodology

The experiments were performed on Ar_2^+ dimers in an ultrahigh-vacuum chamber of COLTRIMS[35,36]. In this methodology, the excitation pulses are followed by the probe pulse, which arrives at a variable delay and dissociates the molecules. The product ions are collected onto a multi-channel plate (MCP) ion detector (Fig. 2c). The 3D momenta and the kinetic energy release (KER) of Ar^+ produced during dissociation of the Ar_2^+ are reconstructed from the times of flight (TOF) and positions of the impacts on the MCP. The estimated vibrational temperature is $T_{vib}=10$ K, so it is safe to assume that the entire population is in the ground state. Details of the molecular beam and of the laser pulses are provided in the Methods.

Under our experimental conditions, the estimated rate of ionization events is much smaller than a single event for each laser shot. At the given laser repetition rate of 10 kHz, the molecules in the interaction volume are refreshed after each laser shot. The COLTRIMS approach, in particular the low event rate and individual particle detection, guarantees that only one molecule is measured at a time. Furthermore, in the rare cases when more than one molecule might have been dissociated, due to the low detection efficiency of the MCP, typically only one Ar^+ fragment is detected, leading, again, to a single-molecule event. Note that if two ionic fragments are detected (extremely rare case), the event is later rejected in the offline data analysis. The Ar^+ ions coming from the dissociation of the Ar_2^+ have a kinetic energy of a few eV and are clearly distinguishable from those coming from ionization of the Ar monomers. The monomer events are therefore excluded based on the kinetic energy of the detected Ar^+.

The interaction of the laser pulses with Ar_2 is depicted in Fig. 2a. The ground electronic state of Ar_2^+ is binding with a dissociation energy of 1.34 eV and equilibrium distance $R_0^+=4.5$ a.u. (ref. [42]), which is smaller than the equilibrium separation of Ar_2 ($R_0=7.2$ a.u.)[43]. The pump pulse at 395 nm creates a vibrational wave packet in the $I(1/2u)$ state of Ar_2^+ centred at the equilibrium distance R_0 (point A) of the neutral Ar_2 dimer. To follow the vibrational dynamics, the wave packet is then dissociated by a time-delayed probe pulse with a delay covering the range of -0.25 ps $< t_p <$ 4.00 ps. The probe pulse at 790 nm 'catches' the oscillating molecule at point B, as illustrated in Fig. 2a, leading to dissociation of Ar_2^+ via $Ar_2^+ \rightarrow Ar^+ + Ar$, denoted as the $Ar_2(1,0)$ channel. The produced Ar^+ fragment has a KER in the range of 0.7 eV $\leq$ KER $\leq$ 1.6 eV.

The measurements are repeated many times for different time delays. The raw data consist of many uncorrelated single events, and for each event the KER and t_p are recorded, giving rise to the functional dependence of KER on t_p. In our experiments, the time delay is scanned with 10 fs resolution. Figure 3c is a result of 40 cycles scanning the whole range of t_p, where each cycle consisted of approximately eight million laser shots, resulting in ~50,000 usable events where one molecule was dissociated and recorded at a time.

Figure 3a–c depicts the gradual build-up of the interference pattern in the KER distribution as more and more events are accumulated. An animated video of this build-up is provided in Supplementary Video 1. The developing interference structure is a time-domain analogue of the build-up of spatial interference fringes while scattering single electrons through a double slit (see ref. [33] and videos therein).

As the pump pulse ionizes a neutral argon dimer, it creates a vibrational wave packet that oscillates on the $I(1/2u)$ potential curve. This wave packet is a superposition of multiple eigenstates of the $I(1/2u)$ potential, as determined by the original equilibrium state of the argon neutral dimer and the laser parameters. The spatial localization of the wave packet persists for several oscillations. However, due to the anharmonicity of the potential, dephasing eventually takes over, leading to the collapse of the wave packet. Figure 3d shows the yield of the $Ar_2(1,0)$ channel as a function of t_p. The curve is obtained by integrating the KER distribution in the range 0.7 eV $\leq$ KER $\leq$ 1.6 eV. The blue curve in Fig. 4b reflects the vibrational motion of the wave packet. The three pronounced oscillations with a period of ~245 ± 10 fs near $t_p=0$ correspond to the initial oscillatory motion of the still localized wave packet on the $I(1/2u)$ potential (Fig. 2a). With the vibrational revival time of Ar_2^+ being 14 ps, the oscillations at doubled frequency near a probe delay of $t_p=3.5$ ps correspond to quarter revival[24,44]. Higher fractional revivals are observed as well, including the 1/8th revival near $t_p=1.8$ ps and the 1/6th revival near $t_p=2.3$ ps. The oscillation period of the 1/8th revival is 63 ± 10 fs and that of 1/6th revival is 82 ± 10 fs.

Observation of echoes in a single molecule

The echo is induced by a kick pulse arriving at $t_k=1.36$ ps after the pump. The kick pulse (395 nm) also couples the $I(1/2u)$ and $II(1/2g)$ states (at point C, Fig. 2a), leading to partial dissociation of the same parent ion with fragments having KER in the range of 2.5 eV $\leq$ KER $\leq$ 3.2 eV, higher than the energy band at 0.7 eV $\leq$ KER $\leq$ 1.6 eV induced by the probe (Fig. 4a). The disjoint KER energy ranges enable unambiguous assignment of each dissociation event to either the probe or the kick pulse. Figure 4b shows the kick-induced (solid green) and probe-induced (solid blue) yields of the $Ar_2(1,0)$ channel as a function of probe delay t_p. The kick perturbs the collapsed wave packet and also partially transfers the population from the $I(1/2u)$ state at point C to the $II(1/2g)$ state, thus triggering the two mechanisms for echo formation discussed already.

In addition to the prominent fractional revivals, the blue curve in Fig. 4b shows three new peaks corresponding to the echo signal (shown in the inset and indicated by arrows at 2.16 ps, 2.41 ps and 2.66 ps). The period of these new oscillations is ~245 ± 10 fs, which is approximately the period of the original oscillations. Thus, the kick has induced a delayed partial rephasing of the original vibrational wave packet. For delays $0 < t_p < t_k$, the probe precedes

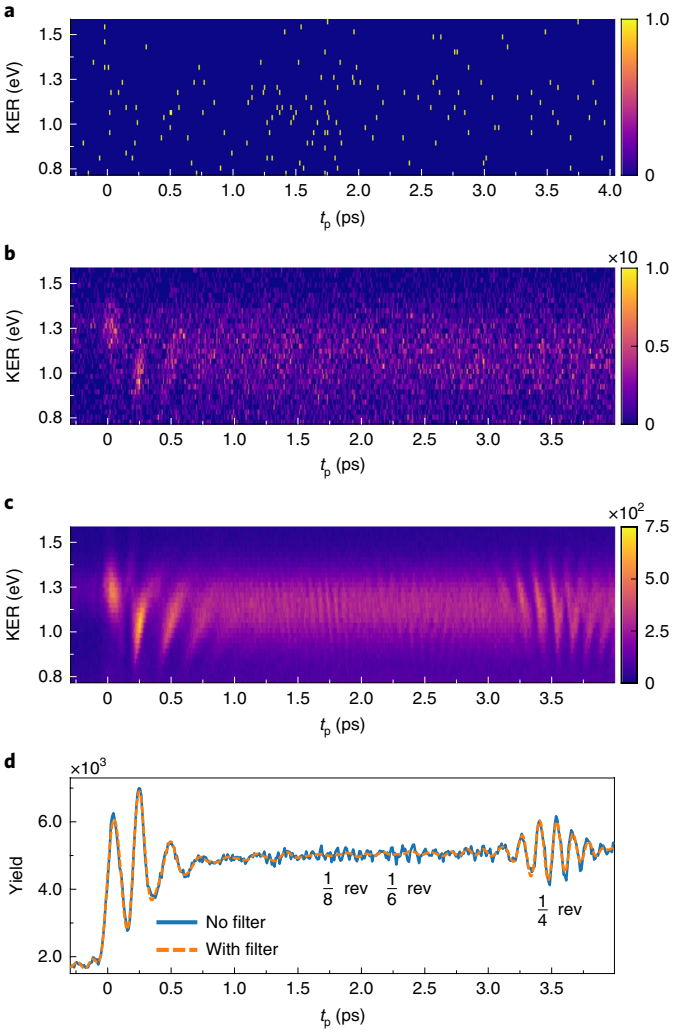

Fig. 3 | KER distribution build-up. a,**b**, Kinetic energy distribution of molecular fragments ($Ar_2(1, 0)$ channel) as a function of the probe delay t_p for 150 accumulated events (**a**) and 1.5×10^4 events (**b**). **c**, The full measurement containing single-molecule events from all 40 cycles (2.0×10^6 events). The colour scales represent the number of events. An instantaneous response to the pulse excitation is clearly visible, as is the quarter revival signal around 3.5 ps. **d**, The yield of the $Ar_2(1, 0)$ channel induced by the probe pulse, shown as a solid blue line. This is obtained by integrating the distribution in **c** over the energy range 0.7 eV ≤ KER ≤ 1.6 eV. The dashed orange curve presents the same data after applying a low-pass filter (see Methods). Here and in the following figures 'rev' denotes revival.

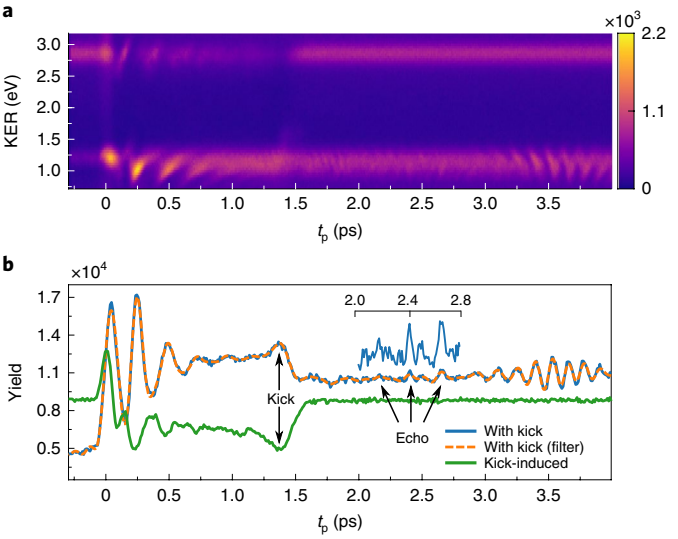

Fig. 4 | KER distribution and yield of the $Ar_2(1, 0)$ channel as a function of the probe delay in the presence of a kick pulse. a, Kinetic energy distribution of molecular fragments ($Ar_2(1, 0)$ channel) as a function of probe delay t_p in the presence of a kick pulse applied at $t_k = 1.36$ ps. The kick at 395 nm produces higher-energy fragments (2.5 eV ≤ KER ≤ 3.2 eV), which are clearly distinguishable from the probe-induced fragments at energies of 0.7 eV ≤ KER ≤ 1.6 eV. **b**, The yield of the probe-induced fragments, shown as a solid blue line. The dashed orange curve shows the same data after applying the low-pass filter (see Methods). The solid green curve shows the kick-induced yield. The probe- and kick-induced yields were obtained by integrating the distribution in **a** over the relevant energy ranges 0.7 eV ≤ KER ≤ 1.6 eV and 2.5 eV ≤ KER ≤ 3.2 eV, respectively.

the kick, so the corresponding kick-induced (green curve) and probe-induced (blue curve) yields of the $Ar_2(1,0)$ channel are out of phase. The drop in the probe-induced yield (blue curve) around $t_p = t_k$ results from the partial depletion of the wave packet by the kick pulse. For longer probe delays $t_p > t_k$, the kick (at a fixed delay of $t_k = 1.36$ ps) precedes the probe and thus the kick-induced yield (green) remains constant.

Although the echo signal partially temporally overlaps the 1/6th fractional revival (around probe delay $t_p = 2.3$ ps), it can be distinguished from the revival by their different oscillation frequencies. Although the oscillation period of the echo signal is the same as that of the original excitation, the frequency of the 1/6th revival oscillations is three times the fundamental frequency. Thus, by applying a low-pass filter, it is possible to significantly suppress the contribution of the 1/6th revival (see Methods). As is shown in Fig. 3d (dashed orange curve), the low-pass filter nearly removes the high-frequency components of the signal, while retaining the contributions of the fundamental and second-harmonic frequencies, increasing the visibility of the echo signal, as displayed in Fig. 4b (dashed orange curve). The magnified part of the curve showing the echo signal is also presented in Extended Data Fig. 1b. The observation of these echoes is the main experimental result of the present work.

Quantum mechanical analysis of the WPE

We carried out quantum mechanical simulations of the observed WPE using two versions of the two-state molecular model (for details see Methods). In the first (simplified) one, we allowed dipole coupling between the $I(1/2u)$ and the $II(1/2g)$ states of Ar_2^+ only for the kick pulse, and calculated the expectation value of the interatomic separation as a function of time, $\langle R \rangle(t)$. These results are used for comparing the quantum WPE in a single molecule, and classical echo in an ensemble of many molecules. In the second, more sophisticated model, both the kick and the probe pulses are allowed to couple the two molecular states. This model fits well the experimental configuration as described above. Here, the probe pulse produces an outgoing wave packet representing the products of dissociation, which is then analysed for constructing the KER spectra as a function of the probe delay. In both versions of the quantum model, we assumed that the initial state is prepared by instantaneous ionization of Ar_2 by the pump pulse; that is, the ground state of the neutral dimer is projected onto the $I(1/2u)$ potential without any change.

The kick pulse acts as a source for both echo-inducing mechanisms—the creation of the 'dynamical hole' (depletion mechanism) and the momentum shift (a.c. Stark shift mechanism). Unlike the classical case, here it is not possible to separate the contributions of

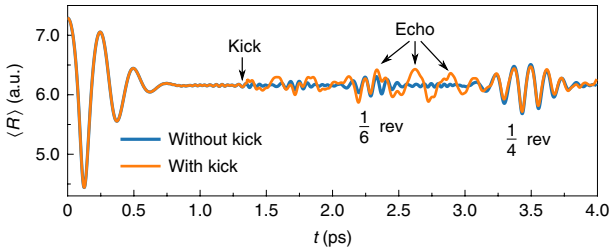

Fig. 5 | Quantum mechanical simulations of the echo dynamics. Expectation value of the interatomic separation $\langle R \rangle(t) \equiv \langle \psi_1 | R | \psi_1 \rangle \langle \psi_1 | \psi_1 \rangle$ as a function of time with (orange curve) and without (blue curve) the kick. This result is calculated without the dissociating probe. The kick transfers ~9% of the population from the ground to the excited ion state. The parameters of the kick pulse are $I_{0k} = 10^{12}$ W cm^{-2}, $\omega_k = 2 \times 0.057$ a.u. (corresponding to 395 nm), $t_k = 1.36$ ps and FWHM$_k$ = 10 fs (FWHM, full-width at half-maximum). The simulations are based on a simplified two-level model, where the initial wave packet is created in the excited state of the Ar_2^+ ion by an instantaneous transfer of the ground-state nuclear wavefunction of the neutral Ar_2 molecule.

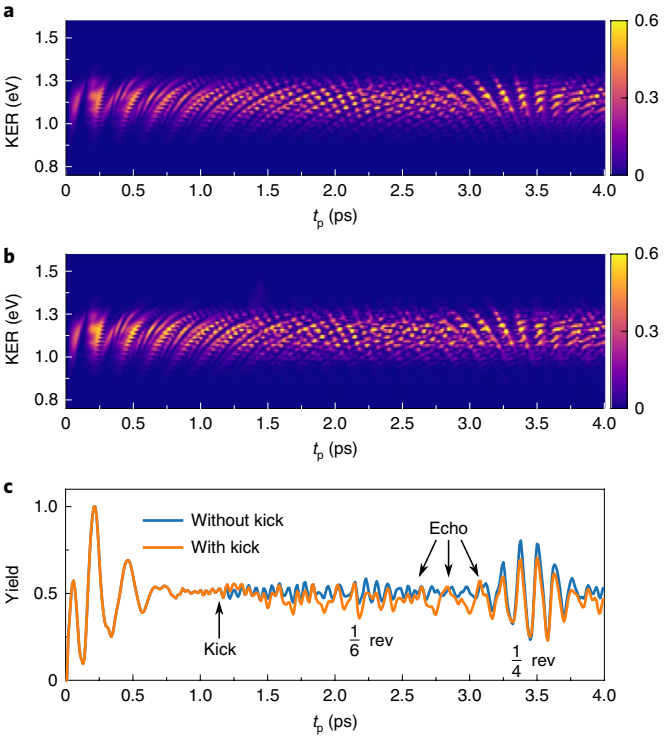

Fig. 6 | KER distributions as a function of probe delay. a,**b**, Kinetic energy distribution of molecular fragments ($Ar_2(1, 0)$ channel) without (**a**) and with (**b**) the kick pulse. The kick arrives at a delay $t_k = 1.36$ ps. **c**, The normalized probe-induced yield of the $Ar_2(1, 0)$ channel as a function of probe delay t_p, with (orange curve) and without (blue curve) the kick pulse. The normalized yield is obtained by integrating the KER distributions (**a**,**b**) in the range of 0.7 eV < KER < 1.6 eV. The parameters of the probe pulse are $I_{0p} = 10^{12}$ W cm^{-2}, $\omega_p = 0.057$ a.u. (corresponds to 790 nm) and FWHM$_p$ = 70 fs. The kick pulse parameters are the same as in Fig. 5.

the momentum shift and depletion, but, as is shown in ref. [41], under the conditions of our experiment the two-state model does include both contributions.

Figures 5 and 6 show the results of the two simulations. Figure 6a,b displays the KER distributions as a function of the probe delay t_p without (Fig. 6a) and with (Fig. 6b) the kick pulse. In analogy to the classical analysis (Fig. 1d,e), both Figs. 5 and 6c show the change in the periodicity of the signal around $t \approx 2t_k$, corresponding to the echo response.

In the experiment, the initial state is generated by the ionizing pump pulse, but this stage is not part of our simulations. The kick pulse gives rise to an echo, which is the main novelty in this work. The probe pulse is used to break the molecules apart and observe the KER. Details of the laser parameters are given in the Methods. The simplified two-level-model quantum simulations successfully emulate the experimentally observed echo signals in the expected time interval. However, a precise quantitative description of the experiment requires more sophisticated modelling that takes into account rotational molecular degrees of freedom (and their coupling to vibrations) and the exact spatiotemporal characteristics of the laser pulses.

Discussion

Here, we introduce WPE in a single isolated molecule and illustrate it in a vibrating argon dimer cation. An analogy is drawn with a related classical echo phenomenon, suggesting impulsive shaking of the molecular potential and impulsive local depletion of the vibrational wave packet as the mechanisms leading to the WPE. However, a proper description requires a full quantum mechanical treatment. In our previous studies on rotational alignment echoes[18], the rotational temperature of the molecules was high enough that the dynamics could be treated classically, but here all the argon dimers are initially in the ground vibrational state and are then prepared in the same pure vibrational wave packet on the ion potential (hence the requirement for quantum treatment).

Recent years have shown increased interest in the coherent dynamics of single quantum objects, especially in relation to storing and retrieving quantum information. Studies on single electron spin echoes in molecular systems[45] and isolated quantum dots[46,47], as well as photon echoes from a few molecules[48], have been reported in the past. In those experiments, as was pointed out by their authors[45–48], the 'single molecule' observations are completely equivalent to the standard echoes observed from an inhomogeneous ensemble of many molecules, with time averages over a single object replacing the ensemble averages. In contrast, in our experiments the entire echo cycle of excitation and observation is completed in an isolated single molecule on an ultrafast timescale.

The present demonstration was carried out on simple dimer molecules, and the method of detection was photon-induced dissociation followed by analysis of the fragments impinging on a time and position detector. Naturally, such a detection method is limited to a relatively small number of particles hitting the detector, and hence to relatively small molecules. However, the phenomenon of WPEs in a single molecule is generic, and with advanced detection methods, one may envisage probing the internal dynamics of larger molecules, shedding light on ultrafast intramolecular processes.

Online content

Any methods, additional references, Nature Research reporting summaries, source data, extended data, supplementary information, acknowledgements, peer review information; details of author contributions and competing interests; and statements of data and code availability are available at https://doi.org/10.1038/s41567-019-0762-7.

Received: 4 April 2019; Accepted: 22 November 2019;
Published online: 20 January 2020

References

1. Hahn, E. L. Spin echoes. *Phys. Rev.* **80**, 580–594 (1950).
2. Hahn, E. L. Free nuclear induction. *Phys. Today* **6**, 4 (1953).

3. Kurnit, N. A., Abella, I. D. & Hartmann, S. R. Observation of a photon echo. *Phys. Rev. Lett.* **13**, 567–568 (1964).
4. Mukamel, S. *Principles of Nonlinear Optical Spectroscopy* (Oxford Univ. Press, 1995).
5. Chebotayev, V. P. & Dubetsky, B. Ya. A classical model of the photon echo. *Appl. Phys. B* **31**, 45–52 (1983).
6. Hill, R. M. & Kaplan, D. E. Cyclotron resonance echo. *Phys. Rev. Lett.* **14**, 1062–1063 (1965).
7. Gould, R. W., O'Neil, T. M. & Malmberg, J. H. Plasma wave echo. *Phys. Rev. Lett.* **19**, 219–222 (1967).
8. Bulatov, A., Kuklov, A., Vugmeister, B. E. & Rabitz, H. Echo in optical lattices: stimulated revival of breathing oscillations. *Phys. Rev. A* **57**, 3788–3792 (1998).
9. Buchkremer, F. B. J., Dumke, R., Levsen, H., Birkl, G. & Ertmer, W. Wave packet echoes in the motion of trapped atoms. *Phys. Rev. Lett.* **85**, 3121–3124 (2000).
10. Herrera, M., Antonsen, T. M., Ott, E. & Fishman, S. Echoes and revival echoes in systems of anharmonically confined atoms. *Phys. Rev. A* **86**, 023613 (2012).
11. Meunier, T. et al. Rabi oscillations revival induced by time reversal: a test of mesoscopic quantum coherence. *Phys. Rev. Lett.* **94**, 010401 (2005).
12. Stupakov, G. *Echo Effect in Hadron Colliders* SSC Report SSCL-579 (SSCL, 1992).
13. Spentzouris, L. K., Ostiguy, J.-F. & Colestock, P. L. Direct measurement of diffusion rates in high energy synchrotrons using longitudinal beam echoes. *Phys. Rev. Lett.* **76**, 620–623 (1996).
14. Stupakov, G. V. in *Handbook of Accelerator Physics and Engineering* 2nd edn (ed. Chau, A. W. et al.) Ch. 2.3.13, 121–123 (World Scientific, 2013).
15. Sen, T. & Li, Y. S. Nonlinear theory of transverse beam echoes. *Phys. Rev. Accel. Beams* **21**, 021002 (2018).
16. Karras, G. et al. Orientation and alignment echoes. *Phys. Rev. Lett.* **114**, 153601 (2015).
17. Karras, G. et al. Experimental observation of fractional echoes. *Phys. Rev. A* **94**, 033404 (2016).
18. Lin, K. et al. Echoes in space and time. *Phys. Rev. X* **6**, 041056 (2016).
19. Lu, J. et al. Nonlinear two-dimensional terahertz photon echo and rotational spectroscopy in the gas phase. *Proc. Natl Acad. Sci. USA* **113**, 11800–11805 (2016).
20. Rosenberg, D., Damari, R., Kallush, S. & Fleischer, S. Rotational echoes: rephasing of centrifugal distortion in laser-induced molecular alignment. *J. Phys. Chem. Lett.* **8**, 5128–5135 (2017).
21. Rosenberg, D., Damari, R. & Fleischer, S. Echo spectroscopy in multilevel quantum-mechanical rotors. *Phys. Rev. Lett.* **121**, 234101 (2018).
22. Eberly, J. H., Narozhny, N. B. & Sanchez-Mondragon, J. J. Periodic spontaneous collapse and revival in a simple quantum model. *Phys. Rev. Lett.* **44**, 1323–1326 (1980).
23. Parker, J. & Stroud, C. R. Coherence and decay of Rydberg wave packets. *Phys. Rev. Lett.* **56**, 716–719 (1986).
24. Averbukh, I. Sh. & Perelman, N. F. Fractional revivals: universality in the long-term evolution of quantum wave packets beyond the correspondence principle dynamics. *Phys. Lett. A* **139**, 449–453 (1989).
25. Robinett, R. W. Quantum wave packet revivals. *Phys. Rep.* **392**, 1–119 (2004).
26. Moerner, W. E. & Kador, L. Optical detection and spectroscopy of single molecules in a solid. *Phys. Rev. Lett.* **62**, 2535–2538 (1989).
27. Orrit, M. & Bernard, J. Single pentacene molecules detected by fluorescence excitation in a p-terphenyl crystal. *Phys. Rev. Lett.* **65**, 2716–2719 (1990).
28. Guenther, T. et al. Coherent nonlinear optical response of single quantum dots studied by ultrafast near-field spectroscopy. *Phys. Rev. Lett.* **89**, 057401 (2002).
29. Unold, T., Mueller, K., Lienau, C., Elsaesser, T. & Wieck, A. D. Optical Stark effect in a quantum dot: ultrafast control of single exciton polarizations. *Phys. Rev. Lett.* **92**, 157401 (2004).
30. Brinks, D. et al. Visualizing and controlling vibrational wave packets of single molecules. *Nature* **465**, 905–908 (2010).
31. Brinks, D. et al. Ultrafast dynamics of single molecules. *Chem. Soc. Rev.* **43**, 2476–2491 (2014).
32. Liebel, M., Toninelli, C. & Van Hulst, N. Room-temperature ultrafast nonlinear spectroscopy of a single molecule. *Nat. Photon.* **12**, 45–49 (2018).
33. Bach, R., Pope, D., Liou, Sy-H. & Batelaan, H. Controlled double-slit electron diffraction. *N. J. Phys.* **15**, 033018 (2013).
34. Aspect, A. & Grangier, P. in *The First Single Photon Sources and Single Photon Interference Experiments* 3–23 (Springer International, 2019).
35. Dörner, R. et al. Cold target recoil ion momentum spectroscopy: a 'momentum microscope' to view atomic collision dynamics. *Phys. Rep.* **330**, 95–192 (2000).
36. Ullrich, J. et al. Recoil-ion and electron momentum spectroscopy: reaction-microscopes. *Rep. Prog. Phys.* **66**, 1463 (2003).
37. De, S. et al. Following dynamic nuclear wave packets in N_2, O_2 and CO with few-cycle infrared pulses. *Phys. Rev. A* **84**, 043410 (2011).
38. Bocharova, I. A. et al. Time-resolved Coulomb-explosion imaging of nuclear wave-packet dynamics induced in diatomic molecules by intense few-cycle laser pulses. *Phys. Rev. A* **83**, 013417 (2011).
39. Lynden-Bell, D. Statistical mechanics of violent relaxation in stellar systems. *Mon. Not. R. Astron. Soc.* **136**, 101–121 (1967).
40. Lichtenberg, A. J. *Phase-Space Dynamics of Particles* (Wiley Series in Plasma Physics, Wiley, 1969).
41. Banin, U., Bartana, A., Ruhman, S. & Kosloff, R. Impulsive excitation of coherent vibrational motion ground surface dynamics induced by intense short pulses. *J. Chem. Phys.* **101**, 8461–8481 (1994).
42. Wüest, A. & Merkt, F. Potential energy curves of diatomic molecular ions from high-resolution photoelectron spectroscopy. I. The first six electronic states of Ar_2^+. *J. Chem. Phys.* **120**, 638–646 (2004).
43. Cybulski, S. M. & Toczyłowski, R. R. Ground state potential energy curves for He_2, Ne_2, Ar_2, He–Ne, He–Ar and Ne–Ar: a coupled-cluster study. *J. Chem. Phys.* **111**, 10520–10528 (1999).
44. Wu, J. et al. Steering the nuclear motion in singly ionized argon dimers with mutually detuned laser pulses. *Phys. Rev. Lett.* **110**, 033005 (2013).
45. Wrachtrup, J., von Borczyskowski, C., Bernard, J., Brown, R. & Orrit, M. Hahn echo experiments on a single triplet electron spin. *Chem. Phys. Lett.* **245**, 262–267 (1995).
46. Koppens, F. H. L., Nowack, K. C. & Vandersypen, L. M. K. Spin echo of a single electron spin in a quantum dot. *Phys. Rev. Lett.* **100**, 236802 (2008).
47. Press, D. et al. Ultrafast optical spin echo in a single quantum dot. *Nat. Photon.* **4**, 367–370 (2010).
48. Dong, H. & Fleming, G. R. Three-pulse photon echo of finite numbers of molecules: single-molecule traces. *J. Phys. Chem. B* **117**, 11318–11325 (2013).

Methods

Molecular beam. Experimentally, a dilute molecular beam was obtained by supersonically expanding argon gas through a 30 µm nozzle into the ultrahigh-vacuum chamber of the COLTRIMS apparatus, under a backing pressure of 1.6 bar. Based on the driving pressure, the temperature of the gas source and the detailed geometry of the jet system, the density of the dimers in the laser beam focal volume was estimated to be 2×10^6 molecules cm^{-3}. For a laser beam diameter at focus of ~7 µm with a Rayleigh length of ~80 µm, there was less than one molecule on average in our laser interaction volume at any given time. The vibrational temperature of the molecules is similar to the translation temperature, which can be estimated using $T_{vib}\approx T_{trans}=\Delta p^2/(4\ln(4)k_B m)$, where k_B is the Boltzmann constant and Δp and m are the FWHM of the momentum distribution in the jet direction and the mass of the singly ionized Ar_2^+, respectively. In our experiment, a momentum width in the jet direction was measured to be $\Delta p\approx5.1$ a.u. for Ar_2^+ cations created by a pump pulse polarized orthogonally to the gas jet. Thus, the vibrational temperature in the interaction region of the argon dimers was estimated to be $T_{vib}=10$ K. At this temperature it is safe to assume that the entire population is initially in the ground molecular vibrational state.

Laser pulses. Three femtosecond pulses were involved in our experiments—pump, kick and probe—all derived from the same Ti:sapphire multi-pass amplifier (790 nm, 25 fs, 10 kHz). Part of the laser beam was frequency-doubled using a beta barium borate (β-BBO) crystal to produce the pump and kick pulses at 395 nm, while the third pulse at the fundamental wavelength of 790 nm was used to dissociate the molecules and probe the vibrational dynamics. The peak intensities of the pulses were 2.0×10^{14} W cm^{-2}, 1.1×10^{13} W cm^{-2} and 8.0×10^{13} W cm^{-2}, and the durations of the pulses (FWHM of the intensity) were 75 fs, 110 fs and 70 fs, respectively. All three laser beams were focused to the interaction region by the same concave mirror inside the chamber. With the high intensity of the pump (2.0×10^{14} W cm^{-2}), most of the neutral dimer molecules within the beam diameter were pumped to the ground Ar_2^+ state. The transverse distribution of the intensity was axially symmetric, and had its maximum at $\rho=0$ (ρ is the distance from the axis of the laser beam). The number of molecules located at distance ρ is proportional to $2\pi\rho d\rho$. Although the ionization probability was maximal at the centre of the focal volume ($\rho=0$), the above geometrical factor reduced the contribution of this area to the measured signal. Most of the yield of the Ar_2^+ ions came from a doughnut-shaped volume (surrounding the propagation axis). For the same reason, by considering the transverse beam profile of the kick and probe pulses and the spatial distribution of the pump-ionization created Ar_2^+, the measured dissociation signal used for observing the echo mainly came from the molecules in the doughnut-shaped volume (where the laser intensity is actually lower than the peak intensity at the beam centre). This focal volume effect explains the usage of lower intensities in our simplified model.

The pulse inducing the echo is the kick pulse. This pulse, at 395 nm, was obtained from the 790 nm/30 fs laser pulses by a β-BBO doubling crystal. The crystal used in the experiment was 0.2 mm thick, so phase matching could not be obtained for the entire incoming bandwidth. Because only part of the spectrum was phase matched, the generated 395 nm pulse was measured to be 40 fs at the exit of the crystal. Furthermore, upon propagation to the focal region to interact with the molecules, the pulse (in fact all pulses) was chirped because of the normal dispersion of the used optical components, leading to unavoidable broadening of the temporal duration of the pulse by keeping the same spectral bandwidth. To assess the temporal duration and chirp of the pulses, we measured the spectrograms of all three pulses in the interaction region using the TG-FROG method[49]. To simulate the dispersion introduced by the window of the vacuum chamber, a piece of glass of the same thickness was included in the beam line before the pulses entered the TG-FROG. The measured linear chirp rates were 900 fs^2, 1,500 fs^2 and 670 fs^2 for the pump, kick and probe pulses, respectively.

Signal filtering. We applied a low-pass filter to the curves in Figs. 3d and 4b. Using a discrete Fourier transform, we obtained the frequency spectrum of the signal containing the fundamental vibration frequency, as well as quarter and 1/6th revival frequencies, denoted f, $2f$ and $3f$, respectively. We then retained only the frequencies below $2f$ in order to remove the 1/6th revival and higher-frequency components. Finally, we reconstructed the signal in the time domain by applying the inverse discrete Fourier transform. Extended Data Fig. 1 shows the magnified portion of Figs. 3d and 4b.

Classical phase space analysis. For the classical simulation, the potential curve was approximated by a Morse potential, $V(R)=D(1-\exp[-a(R-R_0^+)])^2$, where R is the interatomic separation and the parameters are $D=0.048$, $a=0.85$ and $R_0^+=4.56$ (all in atomic units). The three parameters were obtained by fitting the ab initio potential curve[42] with the Morse potential.

Numerical scheme. The time evolution of the two-state system was described by a pair of coupled Schrödinger equations[50,51]:

$$\begin{cases} i\dot{\psi}_1 &= [T+V_1(R)]\psi_1 - E(t)\mu_{\parallel}(R)\psi_2 \\ i\dot{\psi}_2 &= [T+V_2(R)]\psi_2 - E(t)\mu_{\parallel}(R)\psi_1 \end{cases} \quad (1)$$

where T is the kinetic energy operator and indices 1, 2 refer to the $I(1/2u)$ and $II(1/2g)$ potentials ($V_{1,2}(R)$), respectively. The off-diagonal terms describe the dipole coupling between the two states and are equal to the product of the coupling field $E(t)$ and the coordinate-dependent transition dipole moment $\mu_{\parallel}(R)$. In the numerical calculation we add absorbing potentials to the diagonal terms (see below) to avoid spurious reflections from the edge of the spatial grid. The electric fields of the kick and probe pulses are given by

$$E_j(t)=E_{0j}\cos(\omega_j t)\exp\left[-2\ln2\left(\frac{t-t_j}{\mathrm{FWHM}_j}\right)^2\right] \quad (2)$$

where E_{0k}, E_{0p} are the amplitudes of the fields, ω_k, ω_p are the carrier frequencies, t_k, t_p are the delays of the kick and probe pulses, respectively, and $\mathrm{FWHM}_{k,p}$ refers to the temporal intensity profiles of the kick and probe. The coordinate-dependent transition dipole moment of Ar_2^+ is $\mu_{\parallel}(R)=R/2$ (ref. [52]; see below). The coupling field for the first version of the quantum model is $E(t)=E_k$, while for the second it is $E(t)=E_k+E_p$.

For solving the system of coupled Schrödinger equations (equation (1)), we discretize the spatial variable R such that ψ_1 and ψ_2 are represented as column vectors in $\mathbf{C}^N$ and V_1, V_2 are diagonal $N\times N$ matrices, where N is the size of the spatial grid. The discrete fourth-order accurate approximation of the Laplacian operator is given by

$$\frac{\partial^2\psi}{\partial R^2} \approx 12^{-1}(\Delta R)^{-2}[-\psi(R-2\Delta R)+16\psi(R-\Delta R) -30\psi(R)+16\psi(R+\Delta R)-\psi(R+2\Delta R)] \quad (3)$$

and it is represented by a symmetric, sparse $N\times N$ matrix. Here, ΔR is the spatial grid step size and we used $\Delta R=0.15$ a.u. The above form assumes that the wavefunction vanishes at the boundaries, $\psi(R\le R_{min},t)=\psi(R\ge R_{max},t)=0$. To ensure this, we chose the grid size and the total propagation time ($t=t_p+0.3$ ps) such that the probe-induced dissociated wave packet did not reach the boundary by the end of the simulation period. We also included the absorbing potential near the right edge of the spatial grid:

$$V_{abs}=-ia\Theta(R-R_b)\left(\frac{R-R_b}{R_{max}-R_b}\right)^2 \quad (4)$$

Here, $\Theta(\cdot)$ is a unit step function and we used the following parameters: $a=0.01$ a.u., the right grid edge is $R_{max}=34$ a.u. and the beginning of the absorbing layer lies at $R_b=32$ a.u. The absorbing boundary is important when the probe pulse arrives after the kick pulse and the kick-induced outgoing wave packet may have enough time to reach the boundary. The off-diagonal elements of the system (equation (1)) are $E(t)\mu_{\parallel}(R)$. Strictly speaking, the parallel transition dipole moment $\mu_{\parallel}(R)$ equals $R/2$ only for the potentials without the spin–orbit coupling[52]. Nevertheless, we set $\mu_{\parallel}(R)=R/2$, because near the resonance point B (Fig. 2a), $\mu_{\parallel}\approx R/2$. After discretizing the right-hand side of equation (1), an ordinary differential equation solver (based on the fourth-order Runge–Kutta algorithm) was used for time propagation.

KER calculation. To obtain the distribution of the KER as a function of the probe delay, $\xi(\mathrm{KER},t_p)$, we allowed propagation of the wave packet on both $I(1/2u)$ and $II(1/2g)$ potential curves up to $t_{max}=t_p+0.3$ ps for each probe pulse delay t_p and computed the momentum space representation of the wavefunctions at this moment. The integration was carried out in the region $R\in[10,R_{max}]$, where the wave packets representing the dissociation products are well separated from the bound part. Then, the probability density for the kinetic energy was obtained by

$$\xi(\mathrm{KER},t_p)\propto\frac{\sqrt{M}}{p}(|\tilde{\psi}_{I(1/2u)}(p,t_{max})|^2+|\tilde{\psi}_{II(1/2g)}(p,t_{max})|^2) \quad (5)$$

where the $\tilde{}$ denotes Fourier transform.

Data availability

The data represented in Figs. 1, 2b and 3–6 are available through the figshare depository at https://doi.org/10.6084/m9.figshare.10252619.v1. All other data that support the plots within this paper and other findings of this study are available from the corresponding authors upon reasonable request.

References

49. Schmidt, B. E. et al. Poor man's source for sub 7 fs: a simple route to ultrashort laser pulses and their full characterization. *Opt. Express* **16**, 18910–18921 (2008).

50. Garraway, B. M. & Suominen, K. A. Wave-packet dynamics: new physics and chemistry in femto-time. *Rep. Prog. Phys.* **58**, 365 (1995).
51. Magrakvelidze, M. & Thumm, U. Dissociation dynamics of noble-gas dimers in intense two-color IR laser fields. *Phys. Rev. A* **88**, 013413 (2013).
52. Gadea, F. X. & Paidarová, I. Ab initio calculations for Ar_2^+, He_2^+ and He_3^+, of interest for the modelling of ionic rare-gas clusters. *Chem. Phys.* **209**, 281–290 (1996).

Acknowledgements

We acknowledge useful discussions with D. Oron, D. Raanan and G. Stupakov. This work is supported by the National Key R&D Program of China (grant no. 2018YFA0306303), the National Natural Science Foundation of China (grants nos. 11425416, 11834004, 61690224, 11621404 and 11761141004), the 111 Project of China (grant no. B12024), the Israel Science Foundation (grant no. 746/15), the ICORE programme 'Circle of Light', ISF-NSFC (grant no. 2520/17) and Projects from Shanghai Science and Technology Commission (19JC1412200). I.A. acknowledges support as the Patricia Elman Bildner Professorial Chair, and acknowledges the hospitality extended to him by the UBC Department of Physics & Astronomy during a sabbatical stay. This research was made possible, in part, by the historic generosity of the Harold Perlman Family.

Author contributions

J.W., I.A., Y.P., Y.S., J.Q. and I.T. conceived the idea and initiated the study. J.Q., P.L., K.L., W.Z. and F.S. designed and carried out the experiments. I.T. and J.Q. performed the simulations. J.Q., I.T., K.L., J.W., I.A. and Y.P. contributed to the data analysis and writing the manuscript. J.W., I.A. and Y.P. supervised and guided the work.

Competing interests

The authors declare no competing interests.

Additional information

Extended data is available for this paper at https://doi.org/10.1038/s41567-019-0762-7.

Supplementary information is available for this paper at https://doi.org/10.1038/s41567-019-0762-7.

Correspondence and requests for materials should be addressed to Y.P., I.A. or J.W.

Peer review information *Nature Physics* thanks Stefanie Gräfe and the other, anonymous, reviewer(s) for their contribution to the peer review of this work.

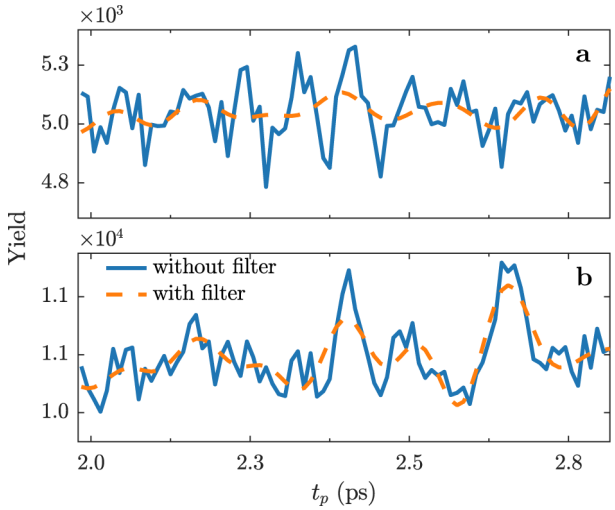

Extended Data Fig. 1 | Magnified parts of Figs. 3d and 4b. a, Yield without the kick pulse. **b**, Yield with the kick pulse. Both curves represent the yield of ion fragments with KER in the range 0.7 eV ≤ KER ≤ 1.6 eV.